Eur. Phys. J. D **22**, 485–493 (2003)
DOI: 10.1140/epjd/e2003-00037-5

THE EUROPEAN PHYSICAL JOURNAL D

Quantum imaging, quantum lithography and the uncertainty principle

Y. Shih[a]

Department of Physics, University of Maryland, Baltimore County, Baltimore MD 21250, USA

Received 30 August 2002 / Received in final form 11 November 2002
Published online 4 February 2003 –

Abstract. One of the most surprising consequences of quantum mechanics is the entanglement of two or more distant particles. Even though we still have questions in regard to fundamental issues of the entangled quantum systems, quantum entanglement has started to play important roles in practical applications. Quantum imaging is one of the hot topics. Quantum imaging has many interesting features which are useful for different applications. For example, quantum imaging can be nonlocal, which is useful for secure two-dimensional information transfer. Quantum imaging can reach a much higher spatial resolution comparing with classical imaging, even beyond the diffraction limit, which is useful for lithography and other microsystem fabrication technology. It is not a violation of the uncertainty principle, however, a quantum mechanical multi-particle phenomenon.

PACS. 42.50.Dv Nonclassical field states; squeezed, antibunched, and sub-Poissonian states; operational definitions of the phase of the field; phase measurements – 42.25.Fx Diffraction and scattering

One of the most surprising consequences of quantum mechanics is the entanglement of two or more spatially distant particles [1]. In a maximally entangled two-particle system, the value of an observable (either space-time or spin observable) for neither single subsystem is determinate (superposition). However, if one of the subsystems is measured to be at a certain value for that observable the other one is 100% determined, *despite the distance between the particles*. In other words, each of the two subsystems may have completely random values, or all possible values, for some physical observable, in the course of its propagation, but when one of them is found to have a certain value in a physical measurement, the value of the other is determined with certainty *immediately* [1].

Even though there are still questions in regarding to fundamental issues of quantum theory, quantum entanglement has started to play important roles in practical engineering applications such as quantum imaging and quantum lithography.

Quantum imaging has many interesting features which are useful for different applications. For example, quantum imaging can be nonlocal, which is useful for secure two-dimensional information transfer. Quantum imaging can reach a much higher spatial resolution comparing with classical imaging, even beyond the diffraction limit, which is useful for lithography and other microsystem fabrication technology.

[a] e-mail: shih@umbc.edu

In this paper, after introducing the concept of quantum entanglement in the first two sections, we review in the following sections two of our recent experiments providing some background understanding of the basic concepts and working principle of quantum imaging and quantum lithography. Brief discussions of the uncertainty principle will be given in the last section.

1 Quantum entanglement

The two-particle entangled state was mathematically formulated by Schrödinger [2]. Consider a pure state for a system composed of two spatially separated subsystems,

$$\hat{\rho} = |\Psi\rangle\langle\Psi|, \quad |\Psi\rangle = \sum_{a,b} c(a,b)\,|a\rangle\,|b\rangle \tag{1}$$

where $\{|a\rangle\}$ and $\{|b\rangle\}$ are two sets of orthogonal vectors for subsystems 1 and 2, respectively, and $\hat{\rho}$ the density matrix. If $c(a,b)$ does not factor into a product of the form $f(a) \times g(b)$ then it follows that the state does not factor into a product state for subsystems 1 and 2:

$$\hat{\rho} \neq \hat{\rho}_1 \otimes \hat{\rho}_2. \tag{2}$$

The state was defined by Schrödinger as the entangled state.

The first classic example of a two-particle entangled state was suggested by Einstein, Podolsky, and Rosen in

1935 [1]:

$$|\Psi\rangle = \sum_{a,b} \delta\left(a + b - c_0\right) |a\rangle\, |b\rangle \tag{3}$$

where a and b are the momentum or the position of particle 1 and 2, respectively, and c_0 is a constant. A surprising feature about the EPR state is the following: *the value of the momentum (position) for neither single subsystem is determinate, i.e., the particle may have any value or all possible values of momentum (position), in the course of its propagation. However, if one of the subsystems is measured to be at a certain value, the value of the other one is determined immediately, despite the distance between the particles.* This point can be easily seen from the delta function in equation (3).

Another classic example of an entangled two-particle system, suggested by Bohm is the singlet state of two spin 1/2 particles [3]:

$$|\Psi\rangle = \frac{1}{\sqrt{2}} \left[|\uparrow\rangle_1 |\downarrow\rangle_2 - |\uparrow\rangle_1 |\downarrow\rangle_2\right] \tag{4}$$

where the kets $|\uparrow\rangle$ and $|\downarrow\rangle$ represent states of spin "up" and spin "down", respectively, along *any arbitrary* direction $\hat{n}$. Again for this state, *the spin for neither particle is determined. It could be "up" or "down" along any direction, or all directions, in the course of its propagation. However, if one particle is measured to be spin up (down) along a certain direction, the other one is determined spin down (up) along that direction immediately, despite the distance between the two spin 1/2 particles.*

2 Two-photon state of spontaneous parametric down conversion

The state of a signal-idler photon pair of spontaneous parametric down conversion (SPDC) [4] is a typical entangled EPR state. SPDC is a nonlinear optical process from which a pair of signal-idler photon is generated when a pump laser beam is incident onto an optical nonlinear crystal. Quantum mechanically, the state can be calculated by the first order perturbation theory [5,6],

$$|\Psi\rangle = \sum_{s,i} \delta\left(\omega_s + \omega_i - \omega_p\right) \delta\left(\mathbf{k}_s + \mathbf{k}_i - \mathbf{k}_p\right) \times a_s^\dagger(\omega(\mathbf{k}_s))\; a_i^\dagger(\omega(\mathbf{k}_i))|0\rangle \tag{5}$$

where $\omega_j, \mathbf{k}_j$ $(j = s, i, p)$ are the frequency and wavevector of the signal (s), idler (i), and pump (p) respectively, ω_p and $\mathbf{k}_p$ can be considered as constants, $a_s^\dagger$ and $a_i^\dagger$ are creation operators for signal and idler photon, respectively.

Figure 1 shows a color picture of the two-photon pair generated from SPDC. The pair is generated in such a way that the energy and momentum of neither one is determinate. Each signal and idler photon may have, simultaneously, all possible colors (energy) and all possible directions (momentum) in the course of its propagation.

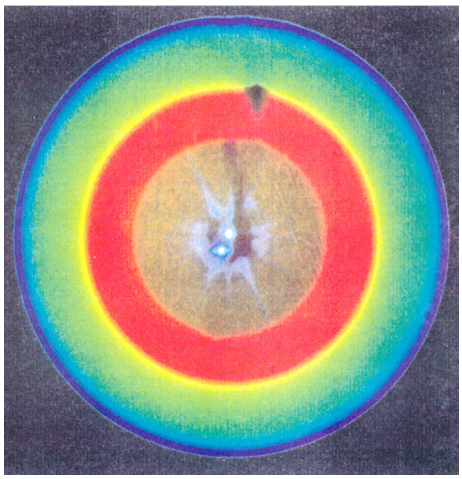

Fig. 1. Photo picture of spontaneous parametric down conversion. The signal and the idler photon can have any color (energy) and can propagate to any direction (momentum). However, if the energy and momentum of one of them is known through a measurement, the energy and momentum of the other is then 100% determined. Experimentally, one can detect a photon at any point on the color "rainbow"; however, if one receives a "click" at a chosen point on the color "rainbow" there is only one unique corresponding point on the opposite side of the "rainbow" to receive its twin by means of a "click-click" coincidence measurement. The scattered light in the center is the "blocked" pump laser beam.

However, if one of them is measured to have certain energy and momentum the energy and momentum of its twin is determined with certainty. It is an entangled two-photon state, but not a state of two individual photons [7]. We have introduced an effective two-photon wavefunction for the signal-idler pair of SPDC, which may be helpful for the understanding of the entanglement nature of the state [5,6].

The two-photon wavepacket or *biphoton* can be calculated according to the standard quantum field theory [8]. The non-factorizable effective two-photon wavefunction $\Psi(t_1, t_2)$ (2-D in configuration space) is calculated to be [5,6,9,10],

$$\Psi(t_1, t_2) = A_0 \mathrm{e}^{-\sigma_+^2 (t_1+t_2)^2} \mathrm{e}^{-\sigma_-^2 (t_1-t_2)^2} \mathrm{e}^{-\mathrm{i}\Omega_s t_1} \mathrm{e}^{-\mathrm{i}\Omega_i t_2} \tag{6}$$

for type-I SPDC [11], where Ω_j, $j = s, i$, is the central frequency for signal or idler, $1/\sigma_\pm$ are "coherence times" associated with the SPDC field (σ_-) and the pump field (σ_+), $t_i \equiv T_i - r_i/c$, $i = 1, 2$, T_i is the detection time of detector i and r_i the optical pathlength from the SPDC to the ith detector. For type-II SPDC [11], the wavepacket $\Psi(t_1, t_2)$, or *biphoton*, is calculated with an *asymmetrical* (with respect to the "zero" of $t_1 - t_2$) rectangular shape,

$$\Psi(t_1, t_2) = A_0 \mathrm{e}^{-\sigma_+^2 (t_1+t_2)^2} \Pi(t_1 - t_2)\; \mathrm{e}^{-\mathrm{i}\Omega_s t_1} \mathrm{e}^{-\mathrm{i}\Omega \mathrm{i} t_2} \tag{7}$$

where

$$\Pi(t_1 - t_2) = \begin{cases} 1 & \text{if } 0 \le t_1 - t_2 \le DL \\ 0 & \text{if otherwise} \end{cases}$$

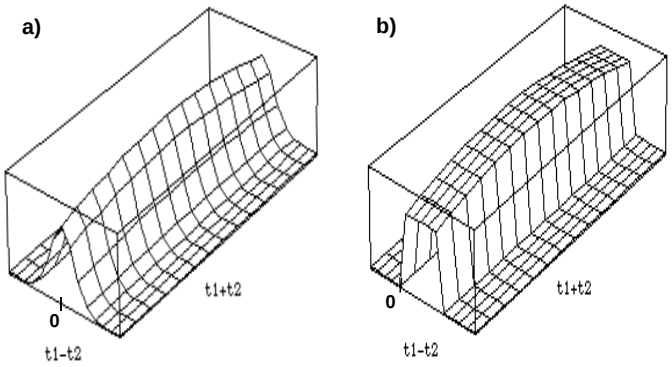

Fig. 2. Two-photon wavepacket envelopes for type-I (a) and type-II (b) SPDC. Note: type-II wavepacket has a rectangular shape in $t_1 - t_2$ and is asymmetric with respect to $t_1 - t_2 = 0$.

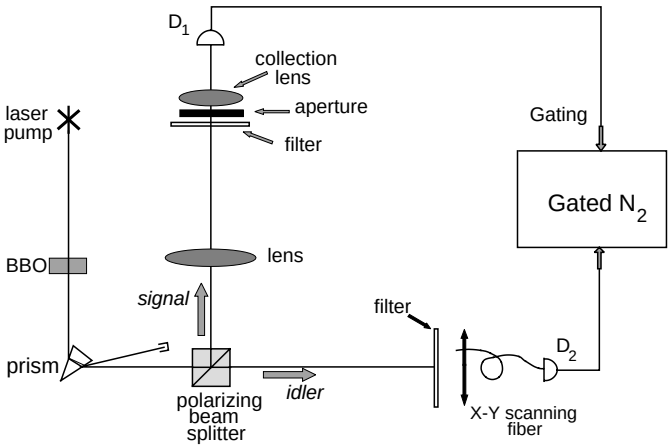

Fig. 3. Schematic setup of the "ghost" image experiment.

and $D \equiv 1/u_o - 1/u_e$, u_o and u_e are recognized as the group velocities of the ordinary and extraordinary rays of the SPDC crystal, and L is the length of the crystal. Figure 2 is a schematic diagram of $\Psi(t_1, t_2)$ for type-I and type-II SPDC, respectively.

The signal-idler photon pair of SPDC has been widely used to prepare EPR-Bohm-Bell states for photon-polarization [12]. The four Bell states which form a complete orthonormal basis are usually represented as,

$$|\Phi_{12}^{(\pm)}\rangle = \frac{1}{\sqrt{2}}\{|0_1 0_2\rangle \pm |1_1 1_2\rangle\},$$
$$|\Psi_{12}^{(\pm)}\rangle = \frac{1}{\sqrt{2}}\{|0_1 1_2\rangle \pm |1_1 0_2\rangle\} \quad (8)$$

where $|0\rangle$ and $|1\rangle$ represent the two orthogonal polarization bases, for example, $|H\rangle$ (horizontal) and $|V\rangle$ (vertical) linear polarization, respectively. In this representation the associated two-photon wavepackets (space-time) has been ignored. However, to prepare Bell states experimentally, it is very important to make the wavepackets "overlapping", *i.e.*, quantum mechanically indistinguishable, to keep the "superposition" in equation (8) valid.

3 "Ghost" image experiment

The first quantum imaging experiment which was done in our laboratory has received the names "ghost" image and "quantum crypto-FAX" by the physics community. These experiments demonstrated the working principle of nonlocal quantum imaging [13].

The schematic of the "ghost" image experimental setup is shown in Figure 3 [13]. The entangled photon pairs are generated from spontaneous parametric down conversion (SPDC) [4]. The 351.1 nm line of an argon ion laser is used to pump a BBO (β-BaB_2O_4) crystal which is cut at a degenerate type-II phase matching angle [11] to produce a pair of orthogonally polarized signal (e-ray of the BBO) and idler (o-ray of the BBO) photon. The pair emerges from the crystal nearly collinear, with $\omega_s \cong \omega_i \cong \omega_p/2$, where ω_j $(j = s, i, p)$ are the frequencies of the signal, idler, and pump, respectively. The pump is then separated from the down conversion by a UV grade fused silica dispersion prism and the remaining signal and idler beams are sent in different directions by a polarization beam splitting Thompson prism. The signal beam passes through a convex lens with a 400 mm focal length and illuminates a chosen aperture (mask). As an example, we have used letters "UMBC" for the object mask. Behind the aperture is the detector package D_1, which consists of a 25 mm focal length collection lens in whose focal spot is a 0.8 mm diameter dry ice cooled avalanche photodiode. The idler beam is met by detector package D_2, which consists of a 0.5 mm diameter multi-mode fiber whose output is mated with another dry ice cooled avalanche photodiode. The input tip of the fiber is scanned in the transverse plane by two encoder drivers. The single and joint detection rates of the two detectors are recorded.

The singles counting rate at each detector is constant. By recording the joint detection counting rates as a function of the fiber tip's transverse plane coordinates, we see the image of the chosen aperture (for example "UMBC"), as is reported in Figure 4. It is interesting to note that while the size of the "UMBC" aperture inserted in the signal beam is only about 3.5 mm × 7 mm, the observed image measures 7 mm × 14 mm. We have therefore managed linear magnification by a factor of 2. Despite the completely different physical situation, the remarkable feature here is that the relationship between the focal length of the lens f, the aperture's optical distance from the lens S_o, and the image's optical distance from the lens (from lens back through beamsplitter to BBO then along the idler beam to the image) S_i, satisfy the Gaussian thin lens equation:

$$\frac{1}{s_o} + \frac{1}{s_i} = \frac{1}{f}\,. \quad (9)$$

In this experiment, we chose $S_o = 600$ mm, and the twice magnified clear image was found when the fiber tip was in the plane of $S_i = 1200$ mm.

It is not difficult to explain this unusual phenomenon according to standard quantum theory. The "ghost" effect

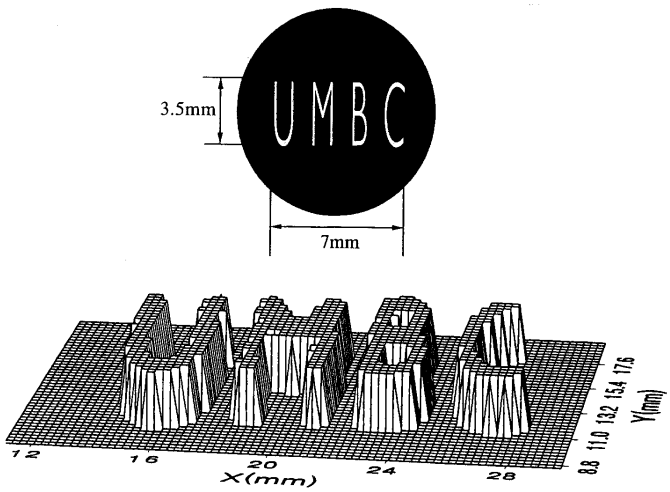

Fig. 4. (a) Upper: a reproduction of the actual aperture "UMBC" placed in the signal beam. (b) Lower: the image of "UMBC": coincidence counts as a function of the fiber tip's transverse plane coordinates. The step size is 0.25 mm. The data shown is a "slice" at the half-maximum value.

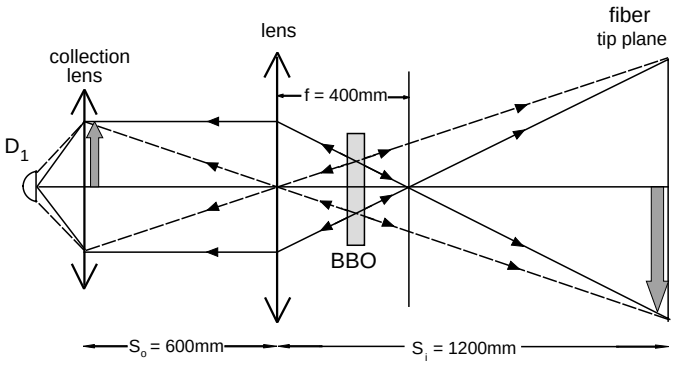

Fig. 5. A conceptual "unfolded" version of the schematic shown in Figure 3, which is helpful for understanding the physics. Although the placement of the lens and the detector obeys the Gaussian thin lens equation, it is important to remember that the geometric rays actually represent pairs of signal-idler photon which propagate in different directions.

is due to the entanglement nature of the two-photon state. The δ functions in equation (5), in the form of energy and momentum conservation, is technically called the phase matching condition:

$$\omega_s + \omega_i = \omega_p, \quad \mathbf{k}_s + \mathbf{k}_i = \mathbf{k}_p. \tag{10}$$

The spatial correlation (position-position) of the signal-idler pair, which encourages two-dimensional imaging applications, is the result of the transverse components of the wavevector phase matching condition (or the momentum-momentum entanglement):

$$k_s \sin \alpha_s = k_i \sin \alpha_i \tag{11}$$

where α_s and α_i are the scattering angles inside the crystal. Upon exiting the crystal, Snell's law thus provides:

$$\omega_s \sin \beta_s = \omega_i \sin \beta_i \tag{12}$$

where β_s and β_i are the exit angles of the signal and idler with respect to $\mathbf{k}_p$ direction. Therefore, in the near degenerate case, the signal-idler pair are emitted at roughly equal, yet opposite, angles relative to the pump, and the measurement of the momentum (vector) of the signal photon determines the momentum (vector) of the idler photon with unit probability and *vice versa*. This then allows for a simple pictorial viewing of the experiment in terms of "usual" geometrical optics in the following manner: we envision the crystal as a "hinge point" and "unfold" the schematic of Figure 3 into that shown in Figure 5. Because of the equal angle requirement of equation (12), we see that all the signal-idler pairs which result in a joint detection can be represented by straight lines (but keep in mind the different propagation directions) and therefore the image is well produced in joint detections when the aperture, lens, and fiber tip are located according to equation (9). In other words, the image is exactly the same as one would observe on a screen placed at the fiber tip if detector D_1 were replaced by a point-like light source and the BBO crystal by a reflecting mirror.

Quantum theory does provide a solution for this unusual "ghost" phenomenon. What we have concluded above is that the signal-idler photon pair can have 100% certainty in both momentum-momentum and position-position correlations. This conclusion may alert us immediately about the uncertainty relations: does it lead to the violation of the uncertainty principle, as EPR and Popper observed [1,14]? Our answer is: no! As a matter of fact, in an entangled two-photon system one could not even have two independent wavepackets, instead one would find a non-factorizable two-dimensional bi-particle wavepacket [5], which is the result of the superposition of the two-photon amplitudes. If there is an uncertainty relation for the entangled two-photon system, it is based on the non-factorizable two-dimensional bi-particle wavepacket but not on the individual single-photon wavepackets.

It should be emphasized that the momentum-momentum correlation and the position-position correlation may be simulated, *separately*, by some classical processes. However, it is impossible to simulate the momentum-momentum and position-position correlation *simultaneously*. Classically, two particles may have a well defined momentum-momentum correlation. For example, by using two co-moving lasers or two co-moving sniper guns one can manage a pair of laser pulses or bullets propagating to certain pre-defined directions. One may place a mask in one path and *project* the mask in the other path by recording the non-blocked (these bullets which pass the mask) pairs pulse by pulse or shot by shot, see detail in reference [15]. However, an optical *projection* is not an *image*. One can never achieve precise position-position correlation at the same time. It would be indeed a violation of the uncertainty principle if one could. The spatial resolution of the projection is basically determined by the size of the laser beam or the size of the bullet of the sniper gun.

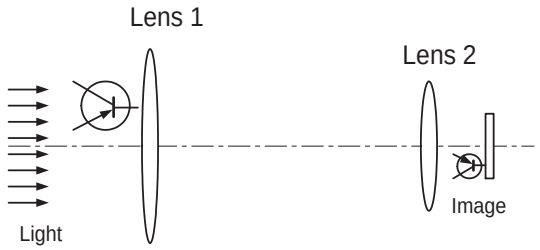

Fig. 6. Schematic of a microscope used for optical lithography. Note: the transistor indicates a complicated lithography pattern, which is used to build up p-n junctions of millions of transistors and other components of an integrated circuit. The demagnified transistor is a "carton" picture of the reduce-sized pattern, which is not in real scale.

One may assume a "zero" size, however, the uncertainty relation will make the spatial resolution even worse.

Once again, in the two-photon system of SPDC, unlike the classical simulation, the momentum for neither signal nor idler is pre-determined before the measurement, *i.e.*, each photon may have *any value and direction* or *all possible values and directions* of momentum, in the course of its propagation. Quantum entanglement is principally different from the pre-determined classical correlation. It is the quantum entanglement that makes it possible to have momentum-momentum and position-position correlation simultaneously. It is the superposition of the two-photon amplitudes determines the spatial resolution of the two-photon imaging. This point can be further seen from next section.

Even though we still have questions in regard to fundamental issues of the entangled quantum systems, quantum entanglement has started to play important roles in practical applications. The above quantum imaging physics lead to an exciting practical application: quantum lithography, which may improve the spatial resolution of an image even beyond the diffraction limit.

4 Diffraction limit – A topic of quantum lithography

Quantum lithography is a topic that has recently attracted much attention [16]. Classical optical lithography technology is facing its limit due to the diffraction effect of light. However, this classical limit can be surpassed, surprisingly, by utilizing the quantum nature of entangled N-photon states. In an idealized experimental situation, the spatial resolution of the lithography imaging can be N times higher than that of the classical limit [17,18].

We have realized a two-photon Young's interference-diffraction experiment recently, which may be considered as a proof-of-principle quantum lithography demonstration [18]. The experiment could be adapted for an N-photon lithography scheme which has the potential to beat the diffraction limit of classical lithography by a factor of N.

Figure 6 shows a schematic picture of a microscope used for lithography. A classical light source is used to make a reduce-sized image of a complicated pattern, for example a lithography pattern for building up p-n junctions of millions of transistors, on the surface of a silicon chip. The resolution of the reduced image cannot be better than half of the wavelength of the classical light source $\lambda/2$, due to the diffraction effect. In other words, to this limit, one cannot reduce the size of the image any more. How to improve the spatial resolution? Classically, the only choice is to reduce the wavelength of the light. However, when the wavelength is too short, for example to the X-ray region, the optical microscope will stop working. There are no effective lenses working at such short wavelengths. Quantum theory provides us another choice: keep the optical wavelength, but make it N-photon entangled state. One would be able to achieve a spatial resolution equivalent of using a classical light with wavelength λ/N.

To demonstrate the quantum lithography idea experimentally, one could compare the spatial resolution of a microscope image by using classical and entangled multi-photon state. It is not an easy job, especially in the case of $N = 2$. To have a clear demonstration, the experiment has to be done in a clever way. What we did was to measure the interference-diffraction pattern of single or double-slit on the Fourier transform plane (or far-field) of a lens. We know that the first lens of a lithography microscope is making a Fourier transform of the "object" and the second lens transforms it back to a reduce-sized image. If one could measure the Fourier transform of the "object" and show that the Fourier transform for the N-photon entangled light of wavelength λ is equivalent to that obtained using a classical light of λ/N instead of λ, one would see immediately that the spatial resolution of the reduce-sized image obtained by the second lens will be N times better. In our recent experiment, we have measured the Fourier transforms of single-slits and double-slits, which are playing the role of the "complicated" pattern for lithography. We found that *under certain experimental conditions*, the two-photon double-slit interference-diffraction pattern has spatial interference modulation period smaller and diffraction pattern width narrower, by a factory of two, than that in the classical case. This result is equivalent to the case of using classical light of wavelength $\lambda/2$. So that the reduce-sized image shall have the potential to beat the diffraction limit of classical lithography by a factor of N.

Figure 7 schematically shows a classical one-dimensional optical diffraction by a single slit. A well collimated laser beam of wavelength λ passes the slit and then its intensity distribution is analyzed in the Fourier transform plane (or in the far-field zone). This distribution, which is the diffraction pattern of a single slit, is well-known to be $\mathrm{sinc}^2(\beta)$, where the parameter $\beta = (\pi a/\lambda)\sin\theta \simeq (\pi a/\lambda)\theta$, a is the width of the slit, and θ is the angle shown in Figure 7 [19]. When β reaches π, the superposition of the wavelets results in a minimum intensity. The $\mathrm{sinc}^2(\beta)$ pattern determines the minimum width one can obtain. Usually, this minimum width is called the "diffraction limit".

To surpass the diffraction limit, our scheme is to utilize the entangled nature of an N-particle system.

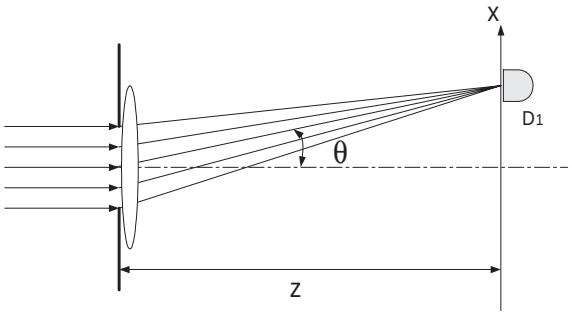

Fig. 7. Classical single-slit diffraction. Zero intensity occurs when the secondary waves ("amplitudes") interfere destructively.

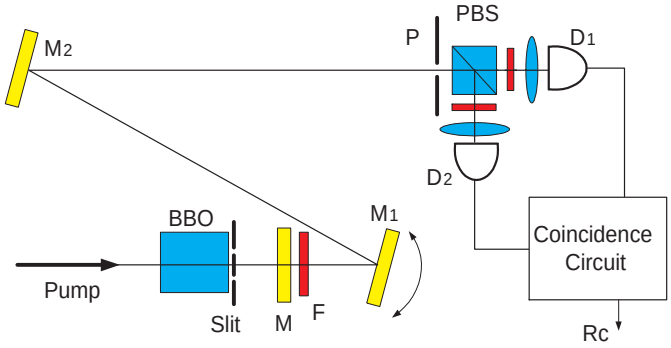

Fig. 9. Schematic of the experimental setup. Details are given in the text.

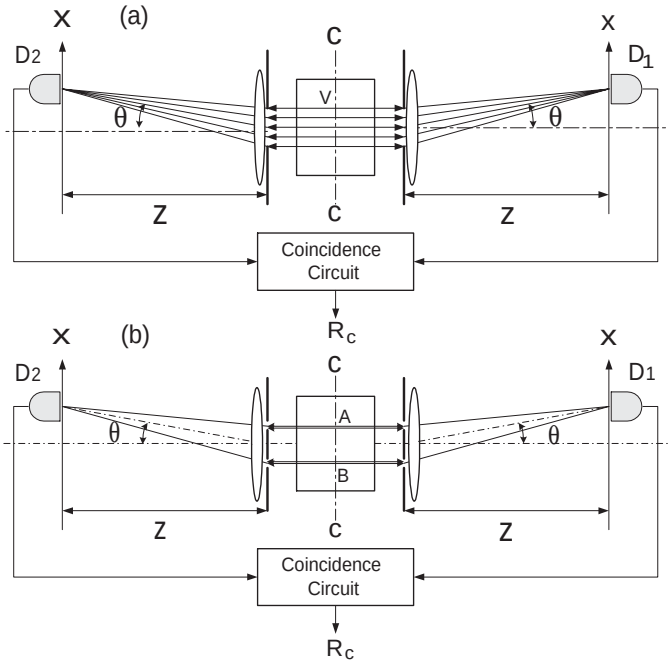

Fig. 8. Schematic of a two-photon diffraction-interference *gedankenexperiment*. The right and left sides of the picture represent signal and idler photons of an entangled pair. Detectors D_1, D_2 perform the joint detection (coincidence) measurement.

To understand the physics of this scheme, consider a *gedankenexperiment* which is illustrated in Figure 8a. An entangled photon pair of wavelength λ can be generated anywhere in region V; however, photons belonging to the same pair can only propagate (1) *oppositely* (momentum entanglement) and (2) *horizontally* (position entanglement; *i.e.*, the pair either pass the upper or the lower slits together) as indicated in the figure. Two slits are placed symmetrically on the left and right sides of the entangled photon source. A photon-counting detector is placed into the far-field zone (or the Fourier transform plane, if lenses are placed following the slits) on each side, and the coincidences between the "clicks" of both detectors are registered. The two detectors are scanning symmetrically, *i.e.*, for each coincidence measurement, both detectors have equal x-coordinates. A two-photon joint detection is the result of the superposition of the two-photon amplitudes, which are indicated in the figure by straight horizontal lines [20]. To calculate two-photon diffraction, we need to "superpose" all possible two-photon amplitudes. Different from the classical case, it is a double integral involving the two slits and the two-photon amplitudes (parallel lines in Fig. 8). The two-photon counterpart of the classical intensity, the joint detection counting rate, is now $\mathrm{sinc}^2(2\beta)$, which gives narrower distribution than the classical pattern by a factor of two. This narrowed pattern is the same diffraction pattern one would observe for wavelength $\lambda/2$. Now if we "fold" the symmetrical left and right sides of the experimental setup together and replace the two independent detectors with a film that is sensitive only to two-photon light (two-photon transition material), then in principle, we have two-photon lithography.

If one replaces the single slit in the above setup with a double-slit, Figure 8b, it is also interesting to see that under the half-width diffraction pattern, the double-slit two-photon spatial interference pattern has a higher modulation frequency, as if the wavelength of the light were reduced to one-half. To observe the two-photon interference, one has to "erase" the first-order interference by reinforcing an experimental condition: $\delta\theta > \lambda/b$ where $\delta\theta$ is the divergence of the SPDC light, b is the distance between the two slits, and λ is the wavelength.

The heart of this *gedankenexperiment* is a special two-photon source: the pair has to be generated in such a desired entangled way as described above; *i.e.*, *precise momentum-momentum and position-position entanglement*. We have found and demonstrated that, *under certain conditions*, the two-photon state generated *via* spontaneous parametric down conversion (SPDC) satisfies the above requirements.

The schematic setup of the experiment is illustrated in Figure 9. It is basically the "folded" version of a double-slit interference-diffraction experiment shown in Figure 8b. The 458 nm line of an argon ion laser is used to pump a 5 mm BBO (β-BaB_2O_4) crystal, which is cut for degenerate collinear type-II phase matching to produce pairs of orthogonally polarized signal (e-ray of the BBO) and idler (o-ray of the BBO) photons. Each pair emerges from the crystal collinearly, with $\omega_s \simeq \omega_i \simeq \omega_p/2$, where ω_j $(j = s, i, p)$ are the frequencies of the signal, idler, and

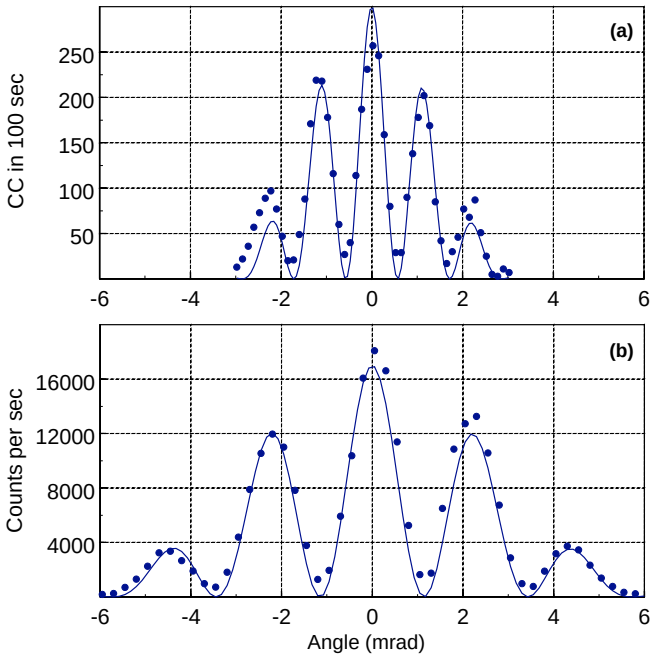

Fig. 10. (a) Experimental measurement of the coincidences for the two-photon double-slit interference-diffraction pattern. (b) Measurement of the interference-diffraction pattern for classical light in the same experimental setup. With respect to the classical case, the two-photon pattern has a faster spatial interference modulation and a narrower diffraction pattern width, by a factor of 2.

pump, respectively. The pump is then separated from the signal-idler pair by a mirror M, which is coated with reflectivity $R \simeq 1$ for the pump and transmissivity $T \simeq 1$ for the signal-idler. For further pump suppression, a cutoff filter F is used. The signal-idler beam passes through a double-slit, which is placed close to the output side of the crystal, and is reflected by two mirrors, M_1 and M_2, onto a pinhole P followed by a polarization beam splitter PBS. The signal and idler photons are separated by the beam splitter and are detected by the photon counting detectors D_1 and D_2, respectively. The output pulses of each detector are sent to a coincidence counting circuit with a 1.8 ns acceptance time window for the signal-idler joint detection. Both detectors are preceded by 10 nm bandwidth spectral filters centered at the degenerate wavelength, 916 nm. The whole block containing the pinhole, PBS, the detectors, and the coincidence circuit can be considered as a two-photon detector. Instead of moving two detectors together as indicated in Figure 8, we rotate the mirror M_1 to "scan" the spatial interference-diffraction pattern relative to the detectors.

One important point to be emphasized is that the double-slit must be placed *as close as possible* to the output surface of the BBO crystal. Only in this case, can the observed diffraction pattern be narrower than in the classical case by a factor of 2.

Figure 10 reports the experimental results. In our experiment, the width of each slit is $a = 0.13$ mm. The distance between the two slits is $b = 0.4$ mm. The distance between the slits and the pinhole P is 4 m. Figure 10a shows the distribution of coincidences versus the rotation angle θ of mirror M_1. The spatial interference period and the first zero of the envelope are measured to be 0.001 and ± 0.003 radians, respectively.

For comparison, we also measured the first-order interference-diffraction pattern of a classical light with 916 nm wavelength by the same double-slit in the same experimental setup, see Figure 10b. The spatial interference period and the first zero of the envelope are measured to be 0.002 and ± 0.006 radians, respectively.

In both "classical" and "quantum" cases, we obtain similar standard Young's two-slit interference-diffraction pattern, $\mathrm{sinc}^2[(\pi a/\lambda)\theta]\cos^2[(\pi b/\lambda)\theta]$; however, whereas the wavelength for fitting the curve in Figure 10b (classical light) is 916 nm, for the curve in Figure 10a (entangled two-photon source) it has to be 458 nm. Clearly, the two-photon diffraction "beats" the classical limit by a factor of 2.

To be sure that we observed the effect of the SPDC photon pair with wavelength of 916 nm but not the pump laser beam with wavelength of 458 nm, we remove or rotate the BBO crystal 90-degree to a non-phase-matching angle and examine the coincidence counting rate. The coincidences remain zero during the 100 second period, which is the data collection time duration for each of the data points, even in high power operation of the pump laser. Comparing this with the coincidence counting rate with BBO under phase-matching, see Figure 10a, there is no doubt that the observation is the effect due to the SPDC.

To explain the result, we have to take into account the quantum nature of the two-photon state of SPDC. Similar to the analysis in the "ghost" imaging experiment, see equations (5, 10–12), in the near degenerate case, the signal-idler pair are emitted at roughly equal, yet opposite, angles relative to the pump, and the measurement of the momentum (vector) of the signal photon determines the momentum (vector) of the idler photon with unit probability and *vice versa*. This then allows for a "unfold" simple pictorial viewing of the experiment as shown in Figure 8.

The coincidence counting rate R_c is given by the probability P_{12} of detecting the signal-idler pair by detectors D_1 and D_2 jointly,

$$\begin{aligned} P_{12} &= \langle \Psi | \, E_1^{(-)} E_2^{(-)} E_2^{(+)} E_1^{(+)} \, | \Psi \rangle \\ &= \left| \langle 0 | \, E_2^{(+)} E_1^{(+)} \, | \Psi \rangle \right|^2 , \end{aligned} \tag{13}$$

where $|\Psi\rangle$ is the two-photon state of SPDC and E_1, E_2 are fields on the detectors. The effect of two-photon Young's interference can be easily understood if we assume for simplicity that signal and idler photons always go through the same slit and never go through different slits. This approximation holds if the variation of the scattering angle inside the crystal satisfies the condition:

$$\Delta\theta \ll b/D, \tag{14}$$

where D is the distance between the input surface of the SPDC crystal and the double-slit. In this case, the state after the double-slit can be written as

$$|\Psi\rangle = |0\rangle + \epsilon\ [a_s^\dagger a_{\rm i}^\dagger \exp({\rm i}\varphi_A) + b_s^\dagger b_i^\dagger \exp({\rm i}\varphi_B)\,]|0\rangle\,, \quad (15)$$

where $\epsilon \ll 1$ is proportional to the pump field and the nonlinearity of the crystal, φ_A and φ_B are the phases of the pump field at region A (upper slit) and region B (lower slit), respectively, and $a_j^\dagger$, $b_j^\dagger$ are the photon creation operators for photons passing through the upper slit (A) and the lower slit (B), respectively. In our experiment, the ratio $(b/D)/\Delta\theta \simeq 30$ and equation (14) is satisfied well enough. Moreover, even the ratio $(a/D)/\Delta\theta$ is of order of 10, which satisfies the condition for observing two-photon diffraction:

$$\Delta\theta \ll a/D. \quad (16)$$

In equation (13), the fields on the detectors are given by:

$$\begin{aligned} E_1^{(+)} &= a_s \exp({\rm i}kr_{A1}) + b_s \exp({\rm i}kr_{B1}) \\ E_2^{(+)} &= a_i \exp({\rm i}kr_{A2}) + b_i \exp({\rm i}kr_{B2}) \end{aligned} \quad (17)$$

where r_{Ai} (r_{Bi}) are the optical path lengths from region A (B) to the ith detector. Substituting equations (15, 17) into equation (13), we get

$$\begin{aligned} R_c \propto P_{12} &= \epsilon^2 \left|\exp({\rm i}kr_A + {\rm i}\varphi_A)\ + \exp({\rm i}kr_B + {\rm i}\varphi_B)\right|^2 \\ &\propto 1 + \cos[k(r_A - r_B)], \end{aligned} \quad (18)$$

where we define $r_A \equiv r_{A1} + r_{A2}$. We have assumed $\varphi_A = \varphi_B$ in equation (18).

In the far-field zone (or the Fourier transform plane), interference of the two amplitudes from equation (15) gives

$$R_c(\theta) \propto \cos^2[(2\pi b/\lambda)\theta]. \quad (19)$$

Equation (19) has the form of a standard Young's two-slit interference pattern, except having the modulation period one-half of the classical case or an equivalent wavelength of $\lambda/2$.

To calculate the diffraction effect of a single slit, we need an integral of the effective two-photon wavefunction over the slit width. Quite similarly to equation (19), it gives

$$R_c(\theta) \propto {\rm sinc}^2[(2\pi a/\lambda)\theta]. \quad (20)$$

Equation (20) has the form of standard single-slit diffraction pattern, except having half of the classical pattern width.

The combined interference-diffraction coincidence counting rate for the double-slit case is given by

$$R_c(x) \propto {\rm sinc}^2[(2\pi a/\lambda)\theta)\cos^2[(2\pi b/\lambda)\theta], \quad (21)$$

which is a product of equations (19, 20).

The experimental observations have confirmed the above quantum mechanical predictions.

One may not see advantages from the above proof-of-principle demonstration. The photon pair is generated in SPDC. So that the pump laser wavelength is one-half of the signal and idler. The improved resolution is the same as that of using the pump laser itself. The advantage, however, is in the case of large number of entangled particle states. One of our approaches is based on our entangled N-photon scheme ($N \geq 3$) [21]. In this approach, one can "beat" the classical limit by a factor of N and still keep the "pump" laser beam wavelength close to one-half that of the entangled photon beam (λ/N *versus* $\lambda/2$).

5 The uncertainty principle

We have concluded from the lithography experiment that the observed entangled two-photon diffraction pattern width is one-half of that of the "classical" light. This conclusion may alert us immediately about the uncertainty relations. What is the uncertainty relation for its momentum Δp_x and its position Δx when a photon passes a single slit of width $\Delta x = a$? In his lecture, Feynman pointed out that it is the same as shown by the diffraction pattern of a "classical" light. Quantitatively, the first minimum of the diffraction pattern reflects the minimum uncertainty relation: $\Delta x \Delta p_x = h$ [22]. The estimation is straightforward.

Considering the classical single-slit diffraction experiment illustrated in Figure 7, the first minimum of the diffraction pattern happens at angle,

$$\beta = \pi = (\pi a/\lambda)\Delta\theta.$$

This lead to,

$$\Delta\theta = \lambda/a,$$

so that,

$$\Delta p_x \simeq p\Delta\theta = (h/\lambda)\Delta\theta = (h/a),$$

so that,

$$\Delta x \Delta p_x = h. \quad (22)$$

It is impossible to produce a "narrower" diffraction pattern by a single photon source, or any classical simulation. Otherwise, the quantum mechanical uncertainty principle would be violated. However, we have observed a diffraction pattern which satisfies $\Delta x \Delta p_x = h/2$ from a two-photon source. Does it mean a violation of the uncertainty relations by a factor of two? Does it mean we are proposing a violation of the uncertainty relations by a factor of N in the case of N-photon entangled state?

The answer is no! What we have observed is not a violation of the uncertainty principle, because of a very simple physics: the entangled two-photon state is not a state of two individual photons. In an entangled two-photon system, one cannot consider each photon individually to "produce" a diffraction pattern and the measurement to show the product of the two. The entangled two-photon

state cannot be factorized as a product, and neither can the diffraction pattern of the two-photon system. The two-photon diffraction pattern is the result of the superposition of the two-photon amplitudes, but not that of the individual subsystems. References [6,23,24] might be helpful for further understanding of the above important physics.

In conclusion, we have shown the possibility of quantum imaging by using two-photon entangled states. The two-photon imaging can be "nonlocal" and can have a spatial resolution beyond the diffraction limit by a factor of two.

References

1. A. Einstein, B. Podolsky, N. Rosen, Phys. Rev. **47**, 777 (1935)
2. E. Schrödinger, Naturwissenschaften **23**, 807 (1935), 823, 844; translations appear in *Quantum Theory and Measurement*, edited by J.A. Wheeler, W.H. Zurek (Princeton University Press, New York, 1983)
3. D. Bohm, *Quantum Theory* (Prentice Hall Inc., New York, 1951)
4. D.N. Klyshko, *Photon and Nonlinear Optics* (Gordon and Breach Science, New York, 1988); A. Yariv, *Quantum Electronics* (John Wiley and Sons, New York, 1989); "Spontaneous Parametric Down Conversion" was called "Spontaneous Fluorescence" and "Spontaneous Scattering" by the pioneer workers
5. M.H. Rubin, D.N. Klyshko, Y.H. Shih, Phys. Rev. A **50**, 5122 (1994); A.V. Sergienko, Y.H. Shih, J. Opt. Soc. Am. B **12**, 859 (1995); Y.H. Shih, A.V. Sergienko, Phys. Rev. A **50**, 2564 (1994)
6. Y.H. Shih, "Two-Photon Entanglement and Quantum Reality", *Advances in Atomic, Molecular, and Optical Physics*, edited by B. Bederson, H. Walther (Academic Press, Cambridge, 1997)
7. T.B. Pittman *et al.*, Phys. Rev. Lett. **77**, 1917 (1996); D.V. Strekalov, T.B. Pittman, Y.H. Shih, Phys. Rev. A **57**, 567 (1998); Y.H. Shih, "Two-Photon Entanglement and Quantum Reality", in *Advances in Atomic, Molecular, and Optical Physics*, edited by B. Bederson, H. Walther (Academic Press, Cambridge, 1997)
8. R.J. Glauber, Phys. Rev. **130**, 2529 (1963); **131**, 2766 (1963)
9. Y.H. Shih, A.V. Sergienko, Phys. Rev. A **50**, 2564 (1994)
10. A.V. Sergienko, Y.H. Shih, M.H. Rubin, JOSA B **12**, 859 (1995)
11. In type-I SPDC, signal and idler are both ordinary (or extraordinary for positive crystal) rays of the SPDC crystal; however, in type-II SPDC the signal and idler are orthogonally polarized, *i.e.*, one is ordinary and the other is extraordinary
12. C.O. Alley, Y.H. Shih, *International Symposium on Foundations of Quantum Mechanics in the Light of New Technology*, edited by M. Namiki *et al.* (Physical Society of Japan, Tokyo, 1986), p. 47; Y.H. Shih, C.O. Alley, Phys. Rev. Lett. **61**, 2921 (1988); Z.Y. Ou, L. Mandel, Phys. Rev. Lett. **62**, 50 (1988); T.E. Kiess *et al.*, Phys. Rev. Lett. **71**, 3893 (1993); P.G. Kwiat *et al.*, Phys. Rev. Lett. **75**, 4337 (1995); Kwiat *et al.*, Phys. Rev. A **60**, R773 (1999); Y.-H. Kim, S.P. Kulik, Y.H. Shih, Phys. Rev. A **62**, 011802(R) (2000)
13. T.B. Pittman, Y.H. Shih, D.V. Strekalov, A.V. Sergienko, Phys. Rev. A **52**, R3429 (1995); D.V. Strekalov, A.V. Sergienko, D.N. Klyshko, Y.H. Shih, Phys. Rev. Lett. **74**, 3600 (1995); two-photon young's double-slit interference type experiment, may not be in the "ghost" format: P.H.S. Ribeiro, S. Padua, J.C. Machado, G.A. Barbosa, Phys. Rev. A **49**, 4176 (1994); A. Zeilinger, Rev. Mod. Phys. **71**, 288 (1996); an overview of the field of quantum imaging: L.A. Lugiato, A. Gatti, E. Brambilla, J. Opt. B **4**, 176 (2002)
14. K.R. Popper, Naturwissenschaften **22**, 48, 807 (1934); K.R. Popper, *From the Postscript to the Logic of Scientific Discovery*, edited by E.I. Bitsakis, N. Tambakis (Gutenberg Publishing, 1984); K. Popper, *Quantum Theory And The Schism In Physics*, edited by W.W. Bartly (Hutchinson, London, 28, 1983); amongst the most notable opponents to the "Copenhagen School" were Einstein-Podolsky-Rosen, de Broglie, Landé, and Karl Popper. One may not agree with Popper's philosophy (EPR classical reality as well) but once again, Popper's thought experiment raises yet another fundamental issue in regard to the foundations of quantum theory
15. R.S. Bennink, S.J. Bentley, R.W. Boyd, Phys. Rev. Lett. **89**, 113601 (2002)
16. A. Eisenberg, New York Times, September 20, (2001)
17. A.N. Boto *et al.*, Phys. Rev. Lett. **85**, 2733 (2000)
18. D'Angelo, M.V. Chekhova, Y.H. Shih, Phys. Rev. Lett. **87**, (2001)
19. See classical optics textbooks, for example, E. Hecht, *Optics*, 2nd edn. (Addison-Wesley Publishing, 1989)
20. D.V. Strekalov, A.V. Sergienko, D.N. Klyshko, Y.H. Shih, Phys. Rev. Lett. **74**, 3600 (1995)
21. T.E. Keller, M.H. Rubin, Y.H. Shih, L.A. Wu, Phys. Rev. A **57**, 2076 (1998)
22. R.P. Feynman, *The Feynman Lectures on Physics*, (Addison-Wesley, Reading, Massachusetts, 1965), Vol. III
23. Y.H. Shih, "Quantum Entanglement and Quantum Teleportation", in *Quantum Theory Centenary*, Ann. Physik **10**, edited by C. Thosmen (Wiley-VCH Publisher, 2000)
24. Y.H. Shih, "Quantum Entanglement: from Popper's Experiment to Quantum Eraser", in *Festschrift in Hornor of Marlan O. Scully*, Opt. Commun. **179**, edited by W.P. Schleich (North-Holland Publisher, 2000)